



24

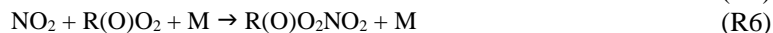
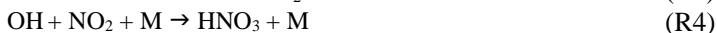
25 **1. Introduction**

26 Tropospheric ozone is a secondary air pollutant formed through a series of reactions
27 involving volatile organic compounds (VOCs) and NO_x (NO_x ≡ NO + NO₂). While
28 tropospheric ozone exists naturally through stratospheric transport (Holton et al., 1995) and *in*
29 *situ* tropospheric production, human activities have drastically perturbed these background
30 values (Lamarque et al., 2005). Exposure to ozone adversely impacts human health, limiting
31 lung and cardiac function, exacerbating chronic respiratory illnesses, and precipitating early
32 mortality (Bell et al., 2006; Park et al., 2005; Jerrett et al., 2009; Silva et al., 2013). In response to
33 these adverse impacts, in 2015 the United States Environmental Protection Agency (EPA)
34 imposed an 8 hour ozone standard of 70 ppbv, lowering the exposure limit from the 75 ppbv
35 standard set in 2008 (EPA, 2015). While ambient concentrations of the ozone precursor NO_x
36 have declined significantly over much of the US (Choi and Souri, 2015; He et al., 2013; Duncan et
37 al., 2016; Lamsal et al., 2015), reductions in ozone concentrations have been less dramatic.
38 Background ozone has actually increased in some locations (Cooper et al., 2012; Choi and Souri,
39 2015); in other areas that have seen decreases in ambient ozone concentrations, such as Texas
40 and the mid-Atlantic region, ozone still periodically exceeds the EPA standard (He et al., 2013).

41 Ozone production is generally classified as either NO_x- or VOC-limited (Kleinman,
42 1994; Thornton, 2002). Net formation of ozone occurs when NO is oxidized to NO₂ by reaction
43 with HO₂ or an organic peroxy radical (RO₂). In the NO_x-limited regime, comparatively low
44 concentrations of NO_x allow for the termination of RO_x (RO_x ≡ OH + HO₂ + RO₂) radicals by
45 self-reactions (e.g. Reactions R1 – R3). In the VOC-limited regime, RO_x radicals are removed
46 from the atmosphere by reactions with NO_x, producing less reactive compounds such as HNO₃
47 (Reactions R4 – R6). In the NO_x-limited regime, reductions in NO_x lead to reductions in O₃;



48 while in the VOC-limited regime, reductions in NO_x without concomitant reductions in VOCs
49 can actually increase O₃ production. One prominent example of this is the weekday/weekend
50 effect in the Southern California Air Basin, where O₃ increases on weekends due to decreases in
51 NO_x emissions from heavy duty diesel trucks (Pollack et al., 2012). The effective
52 implementation of ozone reduction policies therefore requires a detailed understanding of the
53 ozone production regime of the target area.



54
55 Texas is the second most populous state in the US. With multiple large urban centers
56 and a mixture of urban and industrial emissions from petrochemical processing facilities as well
57 as from natural gas and oil extraction, the state has complex pollution chemistry. This
58 combination of a large population and pollution makes understanding ozone production in this
59 region particularly important. Previous studies of ozone formation in Texas have focused
60 primarily on Houston and the surrounding region. Mazzuca et al. (2016) used *in situ*
61 observations of NO_x and O₃ from the DISCOVER-AQ campaign in summer 2013 along with
62 output from the CMAQ model to find significant diurnal variability in ozone production, with
63 higher ozone production rates (P(O₃)) in the morning and a transition from the VOC- to NO_x-
64 limited regime before afternoon. Similar results were found during the TEXAQS2000,
65 TRAMP2006, and SHARP 2009 campaigns (Mao et al., 2010; Ren et al., 2013). Multiple studies
66 have found that anthropogenic alkenes, particularly ethylene and propylene, are major
67 contributors to OH reactivity and therefore O₃ production (Mao et al., 2010; Kleinman et al.,



68 2002; Ryerson et al., 2003) in the region leading to $P(O_3)$ greater than 50 ppbv hr^{-1} (Mazzuca et
69 al., 2016).

70 There have been comparatively few field campaigns, however, to study San Antonio,
71 Texas, the seventh most populous city in the US. In July 2018, the EPA designated the San
72 Antonio region as being in marginal non-attainment with the new 70 ppbv standard, suggesting a
73 need to understand the O_3 formation chemistry in the region. In addition, San Antonio has a
74 significantly different emissions profile than Houston. For example, examination of long-term
75 VOC monitoring in Floresville, TX, a site immediately upwind of San Antonio, suggests that OH
76 reactivity is dominated by alkanes (Schade and Roest, 2016) in contrast with the dominance of
77 alkenes in Houston. Fig. 1 shows the trends in ozone, NO_x , and O_x ($O_x \equiv O_3 + NO_2$) at two
78 Texas Commission on Environmental Quality (TCEQ) monitoring sites, with one (Camp Bullis)
79 located northwest of the urban center and the other (Pecan Valley) in the downtown area (Fig.
80 2b). With the lowering of the 8-hour ozone standard from 75 ppbv (dashed purple line) to 70
81 ppbv (solid purple line), the Camp Bullis site is much more likely to be in exceedance, while the
82 Pecan Valley site remains below both standards. Despite noticeable decreases in maximum NO_x
83 at both sites over the 14-year period shown here, there is little noticeable trend in ozone. This is
84 in agreement with Choi and Souri (2015), who found a $0.07 \times 10^{15} \text{ cm}^{-2} \text{ yr}^{-1}$ decrease in
85 tropospheric column NO_2 over San Antonio between the years 2005 and 2014 while finding an
86 increasing trend of 0.64 ppbv yr^{-1} in the minimum value of surface ozone over the same period.
87 Further study is needed in the San Antonio region to understand the driving factors behind ozone
88 production.

89 In this manuscript, we present results from the San Antonio Field Study (SAFS)
90 conducted in the San Antonio, Texas region in May 2017. We show observations of total peroxy



91 radicals from three sites in the San Antonio area, characterizing the XO_2 ($XO_2 \equiv RO_2 + HO_2$)
92 distribution in the region. We use these XO_2 measurements, along with observations of NO and
93 other trace gas species, to quantify ozone production in regions up- and downwind of the urban
94 core. Though there have been many prior determinations of $P(O_3)$ using measurements of a
95 subset of peroxy radicals (*i.e.*, using laser-induced fluorescence measurements of HO_2 and a
96 fraction of RO_2) (e.g. Ren et al., 2013), this is one of the few determinations of ozone production
97 using the direct observation of total peroxy radicals (Sommariva et al., 2011). Combined with
98 quantification of the primary production of RO_x radicals ($P(RO_x)$) and satellite retrievals of
99 HCHO and NO_2 , we determine the ozone production regime in San Antonio. Finally, we explore
100 the main contributors to OH reactivity in the region.

101 2. Methodology

102 2.1 Campaign Description

103 The SAFS campaign was conducted from 11 to 31 May 2017 at several sites in the
104 greater San Antonio region. We describe measurements made on the Aerodyne Mobile
105 Laboratory (AML) at three sites: the University of Texas San Antonio (UTSA) from 11 to 16
106 May and from 27 to 31 May, Floresville, Texas from 16 to 21 May, and Lake Corpus Christi
107 (Corpus) from 21 to 26 May. The sites were chosen to determine the impact of various emission
108 sources on ozone formation affecting San Antonio. During May in southeastern Texas, the
109 prevailing wind direction is southeasterly, coming off the Gulf of Mexico. UTSA is located
110 northwest (*i.e.* downwind) of downtown San Antonio (Fig. 2a) while the Floresville and Corpus
111 sites were both located upwind of the city. This allows for the determination of background
112 values of compounds through observation at the Floresville and Corpus sites, while observations
113 at UTSA are more representative of air photochemically processed with urban emissions. The



114 AML was situated at all sites to minimize influence from local emissions. At UTSA, the AML
115 was located in a mostly vacant parking lot about 1 km south of the nearest major roadway. In
116 Floresville and Corpus, there were no nearby major roadways, local traffic was at a minimum,
117 and influence from local point and mobile sources was limited. Potential influences from
118 transient local sources (e.g. lawn mowers and jet skis) were removed in the same manner as
119 interference from the generator emissions described below.

120 The AML is outfitted to measure a suite of gas- and particle-phase atmospheric species
121 (Herndon et al., 2005). All instrument inlets were mounted approximately 15 m above ground
122 level on a retractable tower located near the AML. At both the Floresville and UTSA sites, the
123 AML was powered through connection to the local electric utility while at Corpus a diesel
124 generator was used. Although the generator was situated downwind of the instrument inlets,
125 some stagnation and recirculation did occur, allowing for occasional sampling of generator
126 exhaust. Air parcels affected by the generator exhaust were removed through analysis of CO
127 observations. A filter for generator-influenced air was created by determining the minimum CO
128 value over a 100 s period every 5 minutes. Any air parcel with a CO mixing ratio 10 ppbv
129 higher than this minimum was assumed to be impacted by a local transient source, including the
130 generator.

131 Trace gases measured during SAFS and used in this study are summarized here. Unless
132 otherwise indicated, data used in this study were reported as 1-minute averages and then
133 averaged to the 2-minute Ethane CHEMical AMPLifier (ECHAMP) time base, described in the
134 following section. NO₂ was measured at 1 Hz via Cavity Attenuated Phase Shift (CAPS)
135 spectroscopy (Kebabian et al., 2005;Kebabian et al., 2008). Nitric oxide (NO) was measured at
136 0.1 Hz through the same inlet as NO₂ and O₃ using a Thermo Fisher 42i-TL chemiluminescence



137 analyzer, while O₃ was measured with a 2B-Tech model 205 ultraviolet (UV) absorption
138 instrument. Uncertainties (2σ) of the NO, NO₂, and O₃ observations on the ECHAMP
139 measurement time scale are below 5%. The above instruments were zeroed every 15 minutes
140 with humidity-matched zero air. The zero air was generated by passing ambient air through an
141 Aadco ZA30 Catalyst system for VOC removal and through Purafill Chemisorbant Media, a
142 potassium permanganate based scrubber, for NO_x removal.

143 Quantum Cascade – Tunable Infrared Laser Differential Absorption Spectrometers (QC-
144 TILDAS) from Aerodyne Research Inc. were used to measure CO and H₂O (2200 cm⁻¹;
145 measurement wave number), HCHO (1765 cm⁻¹), CH₄ and C₂H₆ (2990 cm⁻¹), H₂O₂ (1277
146 cm⁻¹), and C₃H₈ (2965 cm⁻¹) (McManus et al., 2015). A Proton Transfer Reaction – High
147 Resolution – Time of Flight (PTR-HR-ToF) instrument was used to measure isoprene,
148 acetaldehyde, acetone, benzene, methanol, the sum of monoterpenes, the sum of methyl vinyl
149 ketone (MVK) and methacrolein, and toluene. Finally, a prototype of a commercially-available
150 gas chromatograph from ARI with electron-impact time-of-flight mass spectrometer (GC-EI-
151 ToF-MS) was used to measure a suite of VOCs, including isoprene, 1,2,3-trimethylbenzene,
152 ethyl benzene, cyclohexane, *n*-heptane, *n*-hexane, *n*-octane, *n*-pentane, *o*-xylene, and the sum of
153 *m*- and *p*- xylenes. The GC sampled with a multi-component adsorbent trap (Pollmann et al.,
154 2006) for a 5 minute integration period every 20 minutes. GC observations are unavailable for
155 20-30 May.

156 While there were two independent observations of isoprene, there were limitations with
157 both methods. It was determined that the actual isoprene concentration in the calibration
158 standard used in the field for the PTR had degraded over time, resulting in erroneously high
159 isoprene values. On the other hand, the GC was not calibrated for isoprene during the campaign



160 and observations are only available for half the time. As a result, we use the PTR isoprene from
161 the entire campaign scaled to the GC values, using a GC isoprene sensitivity determined after the
162 campaign. This method results in an estimated isoprene uncertainty of $\approx 30\%$. See the
163 Supplementary Information (SI) for more information.

164 Temperature, wind speed, and wind direction were measured at the top of the inlet tower
165 with a 3D RMYoung (Model 81000RE) sonic anemometer. Atmospheric pressure observations
166 used in this study were taken from the National Weather Service observations at the San Antonio
167 International Airport for the UTSA and Floresville sites and from the Corpus Christi
168 International Airport for the Corpus site. NO_2 photolysis frequencies (J_{NO_2}) were measured via a
169 filter radiometer (MetCon, GmbH) located on top of the AML (Shetter et al., 2003; Stark et al.,
170 2007).

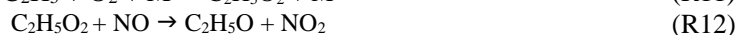
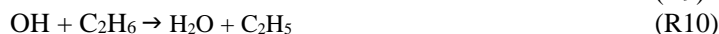
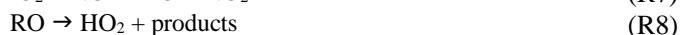
171 2.2 *ECHAMP*

172 Total peroxy radicals (XO_2) were measured via chemical amplification by the ECHAMP
173 instrument. A complete instrument description can be found in Wood et al. (2017), and only the
174 most relevant details are summarized here, including a new sampling system that includes an
175 integrated, remotely-controlled RO_x calibration source. The inlet box is a 39 cm \times 44 cm \times 16
176 cm fiberglass, rainproof electrical enclosure. The box was mounted at the top of the sampling
177 tower and connected to the rest of the instrument via a bundle of tubes and electrical cables.
178 Ambient air was sampled at a flow rate of 6.5 LPM through 76 mm of 3.6 mm inner diameter
179 (ID) glass into the inlet box (see Fig. S1 for a schematic of the plumbing). The glass was
180 internally coated with halocarbon wax to minimize wall losses of XO_2 . The flow was sub-
181 sampled into two, 1.9 cm³ reaction chambers at a flow rate of 1.1 LPM each. Temperature and
182 relative humidity (RH) of the remaining 4.5 LPM of sampled air were measured with a Vaisala



183 probe (Model HMP60). Laboratory tests over a range of flow rates and RH have demonstrated
184 sampling losses of HO₂ of less than 3% and negligible losses of CH₃O₂ [Kundu *et al.*, in
185 preparation].

186 Reaction chambers cycled every minute between an amplification mode and a
187 background mode, for a total cycle time of 2 minutes. In both modes, 25 sccm of 39.3 ppmv NO
188 in N₂ (Praxair) was added at the beginning of the reaction chamber, resulting in a final NO
189 mixing ratio of 0.90 ppmv. In amplification mode, 35 sccm of a 42.2% ethane mixture in N₂
190 (Praxair) was also added to the sampled air at the beginning of the reaction chamber. The radical
191 propagation scheme shown in reactions R7 – R13, in which Reactions (R9) – (R13) repeat
192 numerous times, results in formation of NO₂. The number of NO₂ molecules formed per XO₂
193 molecule sampled is known as the amplification factor (F) and varies with RH. During SAFS, F
194 was 23 for dry air and decreased to 12 at 58% RH. The two calibration methods used to
195 determine F are described below and more fully in the SI. 15.2 cm downstream of the NO/C₂H₆
196 injection point, 35 sccm of N₂ was added to the flow. In the background chamber, the N₂ and
197 C₂H₆ flows were switched (N₂ was added upstream, and C₂H₆ was added downstream), allowing
198 XO₂ radicals to react with NO to form HONO or alkyl nitrates before 35 sccm of the 42.2%
199 ethane mixture was added at the end of the reaction chamber. The resultant NO₂ from each
200 chamber was then measured with separate, dedicated CAPS instruments. Total XO₂ was then
201 determined by the difference between the two NO₂ measurements divided by F.



202



203 The CAPS instruments were calibrated for NO₂ before, after, and once during
204 deployment via quantitative reaction of known concentrations of O₃ generated with a 2B
205 Technologies ozone generator (Model 306) with excess NO. This ozone source agreed within
206 1% with a separate Thermo ozone generation source (Model 49C). All NO₂ calibrations agreed
207 within 5%. The amplification factor (F) was determined by producing known amounts of peroxy
208 radicals by two calibration methods: photolysis of H₂O and of CH₃I. Both methods are described
209 in more detail in the SI. Briefly, the H₂O photolysis method is similar to that used by most HO_x
210 instruments, in which H₂O was photolyzed at a wavelength of 184.9 nm to form an equimolar
211 mixture of OH and HO₂ (Mihele and Hastie, 2000;Faloona et al., 2004). This mixture was then
212 reacted with H₂ to convert the OH into HO₂. Radical concentrations were quantified using the
213 relevant spectroscopic parameters and the measured H₂O and O₃ concentrations in the calibration
214 gas.

215 The second calibration method was based on 254 nm photolysis of CH₃I in humidified
216 air, producing the CH₃O₂ radical. The radical concentration is quantified by reaction of the
217 CH₃O₂ with NO in the absence of C₂H₆, producing 1.86 NO₂ molecules per CH₃O₂. The H₂O
218 photolysis method was performed 6 times, while the CH₃I method was performed once during
219 the field campaign, on 31 May. Both methods were repeated twice in the laboratory after the
220 campaign. Observations from ECHAMP agreed within 12% with the H₂O photolysis calibration
221 source operated by Indiana University during a comparison study in 2015 [Kundu et al., in
222 preparation]. For the XO₂ observations described in this paper, we use the CH₃I calibration.
223 While both methods agree within uncertainty, the H₂O photolysis method was only conducted
224 for RH values of less than approximately 20%, much lower than typical ambient RH. See the SI
225 for further information.



226 The total 2σ accuracy for XO_2 during SAFS was approximately 25%. Calibrations were
227 not performed at RH values greater than 71%. Therefore, we omit all observations with a sample
228 RH greater than 71%. Approximately 85% of these high RH points were observed at nighttime,
229 so we only consider daytime data (7:00 – 20:00 local time) unless otherwise indicated.

230 2.3 Calculation of $P(O_3)$ and $P(RO_x)$

231 We use measurements of XO_2 and NO to calculate the gross rate of ozone production
232 $P(O_3)$ using Eq. (1), in which k_{NO+HO_2} is the reaction constant for the reaction of NO with HO_2
233 and k_i is the reaction constant for NO with an organic peroxy radical $[RO_2]_i$. We note that this is
234 more accurately described as the rate of odd oxygen (O_x) production. Because ECHAMP only
235 measures the sum of peroxy radicals and not their speciation, we assume a simplified form of
236 this relationship (Eq. 2), where k_{eff} is an effective rate constant taken as that of k_{NO+HO_2} . Box
237 modeling results for this site, which will be discussed more fully in a forthcoming paper, show
238 the dominant XO_2 species are HO_2 , CH_3O_2 , and isoprene RO_2 . At 298 K, k_{NO+HO_2} is within 10%
239 of the k values for the reaction of NO with CH_3O_2 and isoprene RO_2 (Orlando and Tyndall,
240 2012), supporting our choice of k_{eff} .

$$P(O_3) = k_{NO+HO_2}[NO][HO_2] + [NO] \sum_i k_i [RO_2]_i \quad (1)$$

$$P(O_3) = k_{eff}[NO][XO_2] \quad (2)$$

241 Similarly, we use the expression shown in Eq. (3) to calculate the primary RO_x
242 production rate. Here, $P(RO_x)$ is the RO_x production rate, J indicates photolysis rate, $k_{O_{1D}+H_2O}$
243 and $k_{O_{1D}+N_2}$ are the reaction constants for the reaction of O_{1D} with H_2O and air, and M is the
244 concentration of $O_2 + N_2$. The Tropospheric Ultraviolet and Visible (TUV) model was used to
245 calculate photolysis rate constants (J values), which were then scaled to the measured J_{NO_2} .
246 HONO was not measured during SAFS. We estimate HONO concentrations assuming an upper



247 limit to the HONO/NO_x ratio of 0.04 as described in Lee et al. (2013). This is an upper bound
248 on the HONO concentration and thus on HONO contribution to P(RO_x). Alkenes, with the
249 exception of the biogenic species isoprene and the sum of monoterpenes, were not measured by
250 the AML during SAFS. Alkene concentrations were estimated from nearby TCEQ monitoring
251 sites, as described in Sect. 3.3. Alkene ozonolysis was calculated to have a negligible impact on
252 P(RO_x) and is omitted from the analysis.

$$P(\text{RO}_x) = 2J_{O_1D}[O_3] \frac{k_{O_1D+H_2O}[H_2O]}{k_{O_1D+H_2O}[H_2O] + k_{O_1D+N_2}[M]} + 2J_{HCHO}[HCHO] + 2J_{CH_3CHO}[CH_3CHO] \quad (3)$$
$$+ J_{Acetone}[CH_3COCH_3] + 2J_{H_2O_2}[H_2O_2] + J_{HONO}[HONO]$$

253 Total P(RO_x) peaks at midday at about 0.65 pptv s⁻¹ on average and is dominated by the ozone
254 and HCHO terms, terms 1 and 2 from Eq. (3), respectively, with contributions from the other
255 observed species totaling less than 5% on average. Contributions from HONO were generally
256 less than 0.1 pptv s⁻¹, even assuming the upper bound in the HONO to NO_x ratio used here.

257 2.4 Satellite Data

258 We use observations of NO₂ and HCHO from the Ozone Monitoring Instrument (OMI) to
259 provide a remotely-sensed estimate of the surface ozone production regime in San Antonio
260 (Duncan et al., 2010; Ring et al., 2018). OMI has a local overpass time of about 13:30 and
261 provides daily, global coverage. The instrument measures backscattered solar radiation in the
262 UV/visible region, allowing for differential optical absorption spectroscopy (DOAS) type
263 retrievals of multiple species, including NO₂ and HCHO.

264 For NO₂, we use the NASA Goddard Space Flight Center (GSFC) version 3 level 2
265 tropospheric column product (Bucsela et al., 2013; Krotkov et al., 2017) gridded to 0.25° latitude
266 × 0.25° longitude resolution. For HCHO, we use the version 3 level 2 reference sector corrected
267 swath product from the Harvard-Smithsonian Astrophysical Observatory (SAO) retrieval



268 (González Abad et al., 2015) also on a 0.25° latitude \times 0.25° longitude grid. For both OMI
269 products, we use only pixels that satisfy quality and row anomaly flags, have a cloud fraction
270 less than 30%, and a solar zenith angle less than 70° . Additionally, data from the two outer most
271 pixels are removed due to their large footprint ($28\text{km} \times 150\text{km}$) compared to the nadir view.

272 We analyze the HCHO to NO_2 ratio using OMI data from May to July 2017. While
273 SAFS lasted only one month, missing data due to cloud cover, the row anomaly, and other
274 factors necessitate a longer time period for data averaging. To calculate the ratio of HCHO to
275 NO_2 , we first calculate the standard deviations (σ) of the HCHO and NO_2 data at each grid point.
276 When calculating the ratio, we only include days within 2σ of the average HCHO and NO_2
277 observations and only include grid boxes that have at least 10 days with coincident observations
278 of both species.

279 **3. Results**

280 **3.1 Distribution of Ozone and its precursors**

281 The highest ozone mixing ratios observed at UTSA were on 14 and 15 May, reaching a
282 maximum near 80 ppbv, while daytime values typically varied between 40 and 60 ppbv during
283 the remainder of the campaign (Fig. 3). Median daytime $[\text{O}_3]$ at all three measurement sites was
284 37 ppbv (Fig. 4a). Median ozone was 18 ppbv higher at UTSA than at the background site in
285 Floresville. Although the highest ozone values were seen at UTSA, there was significant overlap
286 in the ozone distribution between the UTSA and Corpus sites. Consistent with the higher O_3
287 abundance, concentrations of the O_3 precursors isoprene, NO, and XO_2 were also highest at the
288 UTSA site. Median isoprene concentrations, one of the largest contributors to OH reactivity as
289 will be shown later, was almost two orders of magnitude larger at UTSA (1.2 ppbv) than at the
290 other sites (0.05 and 0.03 ppbv at Floresville and Corpus, respectively). While the difference in



291 median [NO] at the sites was not as extreme, a much larger range was seen at UTSA, where the
292 95th percentile of observations was above 2 ppbv. Similar results are seen for the [XO₂]
293 distribution (Fig. 4c), with the highest XO₂ mixing ratios (90 pptv) coinciding with the maximum
294 O₃. Median [XO₂] was approximately a 1.5 times higher at the UTSA site (37 pptv) than at
295 Floresville (26 pptv) and Corpus (25 pptv).

296 XO₂ concentrations showed a distinct diurnal profile (Fig. 5). Overnight values were
297 approximately constant with a median of around 10 pptv, until a small decline after 3:00. A
298 steady increase in [XO₂] began at 9:00, with a peak of 50 pptv at 15:00 and then a decline to the
299 overnight value by 20:00. The shape of this profile is in agreement with other observations of
300 peroxy radicals from a variety of chemical environments (Sanchez et al., 2016; Mao et al.,
301 2010; Whalley et al., 2018). Noise in the nighttime data is a result of higher RH and thus
302 degraded precision of the ECHAMP measurement technique and is not an indication of
303 significant nighttime variability. Even though we have filtered for data points with RH greater
304 than 71% as discussed in Sect. 2.2, nighttime RH is higher than daytime values, on average,
305 decreasing measurement precision. Daytime variability resulted from changes in insolation and
306 biogenic VOC concentrations. The days that showed little or no diurnal profile at UTSA and
307 Corpus were overcast, as evidenced by low J_{NO₂} (Fig. 3). Concentrations of isoprene and the sum
308 of methyl vinyl ketone (MVK) and methacrolein, both isoprene degradation products, were at a
309 maximum when [XO₂] peaked at 90 pptv.

310 The higher O₃ concentrations at UTSA are consistent with its location downwind of the
311 urban core of San Antonio. Figure S2 shows wind roses colored by ozone and the ozone
312 precursors described above. The wind direction while at UTSA was predominantly
313 southeasterly, in agreement with the climatological average for the region. The highest ozone



314 mixing ratios, as well as the highest XO_2 and isoprene, were seen when air parcels originated
315 from this direction, travelling over the city. The highest $[\text{NO}]$ (greater than 2.2 ppbv), however,
316 was seen with northerly and northeasterly winds. This is likely because of the proximity of a
317 major highway north of the UTSA site, which would provide a source of fresher, less processed
318 emissions than in air parcels that travelled from downtown San Antonio. The CO distribution by
319 wind direction (not shown) is consistent with this explanation.

320 *3.2 Ozone production*

321 The highest $\text{P}(\text{O}_3)$ values (and highest $[\text{NO}]$ and $[\text{XO}_2]$) were observed at UTSA. Median
322 $\text{P}(\text{O}_3)$ between 7:00 and 20:00 at UTSA was 4.1 ppbv hr^{-1} , compared to just over 1 ppbv hr^{-1} at
323 both Floresville and Corpus. The 95th percentile, $12.6 \text{ ppbv hr}^{-1}$, is significantly lower than rates
324 found in Houston, which frequently topped 40 ppbv hr^{-1} (Mazzuca et al., 2016; Mao et al., 2010).
325 As with $[\text{O}_3]$ and $[\text{XO}_2]$, the highest $\text{P}(\text{O}_3)$ rates occurred when winds travelled over downtown
326 San Antonio.

327 Figure 6a shows the variation in $\text{P}(\text{O}_3)$ with $[\text{NO}]$, where the data points have been
328 colored by $\text{P}(\text{RO}_x)$ for all observations taken during SAFS. The relationship for the subset of
329 observations exclusively at UTSA is essentially identical. In general, $\text{P}(\text{O}_3)$ increases with
330 $[\text{NO}]$, although a wide range of $\text{P}(\text{O}_3)$ exists for a given value of NO. For a constant value of
331 $[\text{NO}]$, $\text{P}(\text{O}_3)$ is consistently higher at higher $\text{P}(\text{RO}_x)$. Figure 6b shows the same data as panel a
332 but binned both by NO mixing ratio and $\text{P}(\text{RO}_x)$. All $\text{P}(\text{O}_3)$ observations have been separated
333 into NO bins with an equal number of observations, as well as into two bins of $\text{P}(\text{RO}_x) < 0.15$ and
334 $\text{P}(\text{RO}_x) > 0.5$. The values of $\text{P}(\text{RO}_x)$ were chosen to represent the low and high ranges of $\text{P}(\text{RO}_x)$
335 observed during SAFS. The conclusions drawn from the results are insensitive to the values
336 chosen for these bins.



337 Figure 6b demonstrates that the majority of observations made during SAFS were in the
338 NO_x -limited regime. For the high $P(\text{RO}_x)$ observations, there is a steady increase in $P(\text{O}_3)$ up to
339 the 500 pptv NO bin. Above this point, $P(\text{O}_3)$ potentially plateaus, but there were insufficient
340 observations at higher NO to determine the location of the turnover point in ozone production.
341 Because the majority of NO observations at UTSA were less than 500 pptv, we conclude that the
342 site is predominantly NO_x -limited. Further observations at higher NO mixing ratios are required
343 to determine the turnover point for ozone production in this region. For the low $P(\text{RO}_x)$ case,
344 there is a peak in $P(\text{O}_3)$ at 200 pptv NO, suggesting that in a low $P(\text{RO}_x)$ environment, UTSA
345 can be VOC-limited at higher NO mixing ratios. Because $P(\text{O}_3)$ is typically only 1 ppbv hr^{-1}
346 when $P(\text{RO}_x)$ is at these levels, however, ozone production in this regime is negligible. For the
347 NO_x -limited points, increases in VOC concentrations are expected to have a small impact on
348 $P(\text{O}_3)$; for the VOC-limited points, increases in VOCs will lead to increased $P(\text{O}_3)$. The true
349 turnover concentration for NO cannot be easily inferred by inspection of a graph of $P(\text{O}_3)$ versus
350 $[\text{NO}]$, however, because VOC concentrations are not constant for all points. Additional analysis
351 does suggest that the majority of the observations during SAFS were in the NO_x -limited regime.

352 These results are consistent with the diurnal profile of the ozone production regime as
353 determined by the separate " L_N/Q " metric, which is the ratio of the RO_x loss rate due to reactions
354 with NO_x (e.g., R_3) to the total RO_x loss rate (Q) (Kleinman, 2005). In general, when more than
355 half of the RO_x loss is due to reaction with NO_x species ($L_N/Q > 0.5$) then $P(\text{O}_3)$ is VOC-
356 limited, whereas when the majority of RO_x loss is due to peroxy radical self-reactions ($L_N/Q <$
357 0.5) $P(\text{O}_3)$ is NO_x -limited. The Framework for 0-Dimensional Atmospheric Modeling (F0AM)
358 photochemical box model (Wolfe et al., 2016b), constrained to observations, was used to model
359 the parameters needed to calculate L_N/Q at the SAFS sites. A full description of the model setup



360 is in the SI. Using the box model results and the method described in Kleinman (2005), we
361 calculated L_N/Q for all box-modeled observations at UTSA (Fig. 7). A clear diurnal pattern is
362 evident with an early morning maximum and then a quick decline to $L_N/Q < 0.5$ at 9:00, after
363 which the ratio remains below 0.1 for the remainder of the day. At 18:00, however, the ratio
364 does begin to increase, though remaining well in the NO_x -limited space. While L_N/Q is highest
365 in the morning, $P(\text{O}_3)$ is at a minimum during this time period, suggesting that there is little O_3
366 production when $P(\text{O}_3)$ is VOC-limited. Furthermore, time periods where ozone was found
367 under VOC-limited conditions were likely confined to a relatively small volume of air in the
368 shallow, morning boundary layer. This transition from VOC- to NO_x -limited between morning
369 and afternoon is consistent with other locations (Mazzuca et al., 2016; Mao et al., 2010; Ren et al.,
370 2013) and the high NO concentrations that build up in the morning from local traffic and a low
371 boundary layer.

372 Finally, remotely sensed observations of NO_2 and HCHO from the OMI satellite
373 corroborate the conclusion that ozone production in San Antonio is NO_x -limited. The ratio of
374 column HCHO to tropospheric column NO_2 has been used as an indicator of the ozone
375 production regime in multiple regions (Duncan et al., 2010; Ring et al., 2018). According to
376 Duncan et al. (2010), a region is considered NO_x -limited when this ratio is greater than 2, VOC-
377 limited for values less than 1, and in a transition region for ratios between 1 and 2. Other studies
378 dispute these ranges, claiming that, in Houston, the NO_x -limited regime only begins for a ratio
379 greater than 5 (Schroeder et al., 2017). Figure 2 shows the ratio averaged over the months May –
380 July 2017 over Texas. In agreement with the *in situ* observations and the above analysis, the
381 satellite data places all three locations in the NO_x -limited regime with ratios much greater than 5.
382 Though they provide much higher spatial coverage, polar orbiting satellite observations are



383 limited in that they provide coverage once daily and that data must be averaged over a long
384 period to gain meaningful statistics. Likewise, because of the satellite footprint, any small
385 regions in urban centers that may be VOC-limited might not be evident here because of spatial
386 averaging. Nevertheless, the combination of satellite and *in situ* observations clearly
387 demonstrates that, at least at the three measurement sites, ozone production was NO_x-limited.

388 **3.3 OH Reactivity**

389 In contrast with Houston, the OH reactivity, and thus ozone production, at the UTSA
390 measurement site was driven by biogenic species, particularly isoprene. Figure 8 shows the OH
391 reactivity for the UTSA and Floresville sites. Observations after 19 May were excluded because
392 of the lack of GC observations. OH reactivity is defined as the sum of the products of the
393 reaction rate coefficient of a species with the concentration of that species (Eq. 4).
394 Concentrations of all observed OH reactive species were used to calculate the total OH
395 reactivity. These values were then divided into 5 groups: biogenics (isoprene, MVK,
396 methacrolein, and α -pinene), carbonyls (HCHO and acetaldehyde), alkanes (ethane, propane,
397 cyclohexane, octane, heptane, hexane, and pentane), NO_x, CO, CH₄, O₃, and other (benzene,
398 1,2,4-trimethylbenzene, ethyl benzene, toluene, *o*-, *p*-, and *m*-xylene, methanol, and C₂H₂). With
399 the exception of isoprene and monoterpenes, alkenes were not measured onboard the AML. To
400 estimate the impact of anthropogenic alkenes on OH reactivity, we include observations from
401 nearby TCEQ monitoring sites, Camp Bullis for UTSA and a site in Floresville co-located with
402 the AML. These sites provide hourly observations of alkenes, including *cis*-2-butene, *trans*-2-
403 butene, 1-pentene, *cis*-2-pentene, *trans*-2-pentene, ethene, propene, 1,3-butadiene, and 1-butene.
404 Comparison of alkanes measured onboard the AML to those measured at the Camp Bullis TCEQ
405 site shows only marginal agreement, suggesting that alkene concentrations used here might also



406 differ between the SAFS and TCEQ sites. In any case, the inclusion or omission of these alkene
407 observations from the TCEQ sites has almost no effect on the results. Alkenes contribute less
408 than 1% of total reactivity at both UTSA and Floresville for morning and afternoon times, so we
409 do not include them in our discussion below.

$$k_{OH} = \sum_i k_{(X+OH)}[X]_i \quad (4)$$

410

411 OH reactivity varied substantially at the two sites in both magnitude and relative
412 importance of the individual constituents. Overall, average afternoon OH reactivity at UTSA
413 and Floresville were 12 and 4.0 s⁻¹, respectively. While the main contributors to OH reactivity
414 varied between morning and afternoon at both sites, the total reactivity did not show significant
415 variation. The higher OH reactivity at UTSA is consistent with the higher P(O₃) rate and XO₂
416 concentrations. At UTSA, the predominant contributors to OH reactivity were NO_x in the
417 morning and biogenic VOCs in the afternoon, comprising 46% and 55% of OH reactivity,
418 respectively. Isoprene dominated the biogenic contribution, with less than 10% of total OH
419 reactivity resulting from monoterpenes, which have been assumed to be 100% α-pinene.
420 Although the contribution of biogenic VOCs was lower at Floresville than at UTSA, they were
421 still the largest component of OH reactivity in the afternoon. The significant contribution to OH
422 reactivity from NO_x during the morning is consistent with large on-road emissions and a low
423 boundary layer as well as with the VOC-limited nature of O₃ production in the morning. CO and
424 carbonyls were the other major contributors to OH reactivity at all locations, with CO being the
425 dominant contributor at Floresville in the morning. Because one of the dominant contributors to
426 HCHO production is isoprene (Wolfe et al., 2016a), it is likely that the biogenic contribution to



427 OH reactivity is even higher than indicated here. Contributions from alkanes were unimportant
428 at the UTSA site and contributed only 4-5% at Floresville.

429 The uncertainty in the isoprene measurements does not significantly alter the conclusions
430 presented here. To bound the effect of this uncertainty, we adjusted the isoprene observations by
431 $\pm 32\%$ and recalculated the OH reactivity. This results in a range of 10.5 – 13.4 and 3.8 – 4.3
432 s^{-1} in total afternoon OH reactivity at UTSA and Floresville, respectively. NO_x remains the
433 dominant contributor at UTSA in the morning. For the lower bound, isoprene contributes 49%
434 of total OH reactivity at UTSA, by far the largest contributor to afternoon OH reactivity, and
435 23% at Floresville, making it second in importance to CO (25%).

436 **4. Discussion and conclusions**

437 We have presented observations of O_3 , its precursors, and total observations of XO_2 at
438 three sites in the San Antonio region. We also presented determinations of $\text{P}(\text{O}_3)$ calculated from
439 measurements of total peroxy radicals. During SAFS, ozone peaked at UTSA at 80 ppbv, with a
440 median value of 47 ppbv, almost 20 ppbv higher than at the background site of Floresville,
441 upwind of San Antonio. Along with higher O_3 , the UTSA site also had larger $\text{P}(\text{O}_3)$, isoprene,
442 NO, and XO_2 concentrations than upwind sites. Differences in $[\text{O}_3]$ between the up- and
443 downwind sites could be the result of the effects of urban emissions on O_3 production, or they
444 could result from daily variability, since simultaneous observations were not made at both sites
445 and there are no permanent O_3 observations at Floresville. Figure S3 compares O_3 observations
446 from the AML while at UTSA to those made by the University of Houston (UH), who measured
447 O_3 continuously at UTSA during SAFS, and to observations from the TCEQ site at Lake
448 Calaveras, located upwind of downtown San Antonio (Fig. 2b). Between 17 and 30 May, winds
449 in the San Antonio region were primarily southeasterly (*i.e.* they travelled in the general



450 direction from Lake Calaveras to UTSA, with downtown San Antonio in-between). During this
451 period, there are both days where O_3 is almost identical at both sites and where O_3 is 20 ppbv
452 higher at UTSA, suggesting significant O_3 production in the air as it travelled between the two
453 sites. These results suggest that the 20 ppbv differences in median values between the UTSA
454 and Floresville sites could be either the result of day-to-day variability, *in situ* O_3 production as
455 the air travelled between the two sites, or a mixture of the two. Further observations of O_3 and
456 its precursors in the region, including in downtown San Antonio, are needed to fully characterize
457 the effects of the city on ozone production.

458 A variety of methods were used to show that with the exception of early morning, when
459 NO is high and XO_2 concentrations are low due to limited insolation, ozone production at the
460 three SAFS sites is NO_x -limited. These results are limited to the examined time period and
461 location, but comparison to O_3 and NO levels at the Camp Bullis site suggests the observations at
462 UTSA are typical for an area downwind of the San Antonio urban center. This is in contrast,
463 however, to observations at the TCEQ Pecan Valley site which has not had an ozone exceedance
464 day by either EPA standard since 2015 but regularly has MDA8 NO greater than 50 ppbv,
465 significantly larger than the maximum 2-minute value of 4 ppbv seen at the UTSA site. Mixing
466 ratios of O_x at Pecan Valley and Camp Bullis (Fig. 1) are essentially identical, suggesting that
467 there is less O_3 titration downwind of central San Antonio than in the urban core. Given the
468 higher $[NO_x]$ in the urban core of San Antonio, $P(O_3)$ could be significantly different than at the
469 UTSA site.

470 OH reactivity at UTSA was found to be 12 s^{-1} , with the primary contributor being
471 isoprene. While the overall magnitude of the reactivity was comparable to that observed and
472 modeled during the TRAMP2006 campaign in Houston (Mao et al., 2010), the contributors to



473 OH reactivity were found to be significantly different. Contributions from aromatics were
474 negligible at UTSA while they were found to be 15% during TRAMP2006. In Houston,
475 anthropogenic alkenes were found to be responsible for 20-30% of total reactivity, with biogenic
476 VOCs making up less than 10%. Here, biogenic VOCs were responsible for 55% of total
477 daytime reactivity, with alkenes making up less than 1%, although alkene values were based on
478 estimates from a different site. We caution that this result cannot necessarily be extrapolated to
479 other areas in the San Antonio region. Isoprene has a lifetime on the order of an hour, and the
480 high biogenic contribution to OH reactivity seen here could result from a chemical environment
481 at UTSA that differs from the rest of San Antonio. Further observations are needed to confirm
482 that this is true for the entire region. Schade and Roest (2016) found a significantly different OH
483 reactivity profile at Floresville than described here, with alkanes accounting for approximately
484 70% of total OH reactivity, with biogenic VOCs contributing less than 5%. They report
485 statistics for yearly data of individual species concentrations from 2013 to 2014, so direct
486 comparisons are difficult. Observed isoprene at Floresville during SAFS was more than an order
487 of magnitude larger than that reported in Schade and Roest (2016), with alkane concentrations
488 consistent between the two studies. Differences in reactivity could result from differences in
489 biogenic emissions as well as in differences in anthropogenic emissions, as fossil fuel production
490 in the Eagle Ford Shale region (outlined in Fig. 2) has declined recently. Nevertheless, these
491 results suggest that policies designed to limit O₃ production at the SAFS sites discussed here
492 should initially focus primarily on NO_x reductions as the region is NO_x limited and the primary
493 VOC contributor is biogenic. Further observations and analysis are need to determine whether
494 this holds true in the urban core of downtown San Antonio.

495 **5. Data Availability**

496



497 Data from SAFS are maintained on a private server but are available upon request to the
498 authors.

499

500 **6. Author Contributions**

501

502 D.C.A. and E.W wrote the manuscript. All authors discussed the results and commented
503 on the manuscript. All authors also contributed to daily running of the AML. S.C.H. led the
504 campaign. D.C.A., J.P, and E.C.W. measured XO₂. B.M.L. and W.B.K. contributed to the
505 measurement of organic trace gases. J.R.R., T.I.Y., and S.C.H. led observations with TILDAS
506 instruments as well as measurements of NO, NO₂, and O₃.

507

508 **7. Competing Interests**

509

510 The authors declare no competing interests.

511

512 **8. Acknowledgements**

513

514 The authors acknowledge support from NSF grants AGS-1443842 and AGS-1719918. In
515 addition, this research was funded by a grant (project 17-032) from the Texas Air Quality Research
516 Program (AQRP) at the University of Texas Austin through the Texas Emission Reduction Program
517 (TERP) and the Texas Commission on Environmental Quality (TCEQ). The findings, opinions, and
518 conclusions are the work of the authors and do not necessarily represent the findings, opinions, or
519 conclusions of the AQRP or the TCEQ. The authors thank S. Hall and K. Ullmann of NCAR, J. Flynn of
520 the University of Houston, D. Sullivan of the University of Texas at Austin, and R. Nadkarni and M.
521 Estes of TCEQ for their contributions to the SAFS campaign and this paper.



522

523 **9. References**

524

525 Bell, M. L., Peng, R. D., and Dominici, F.: The exposure-response curve for ozone and risk of
526 mortality and the adequacy of current ozone regulations, *Environmental Health Perspectives*,
527 114, 532-536, 10.1289/ehp.8816, 2006.

528 Bucsela, E. J., Krotkov, N. A., Celarier, E. A., Lamsal, L. N., Swartz, W. H., Bhartia, P. K.,
529 Boersma, K. F., Veeffkind, J. P., Gleason, J. F., and Pickering, K. E.: A new stratospheric and
530 tropospheric NO₂ retrieval algorithm for nadir-viewing satellite instruments: applications to
531 OMI, *Atmos. Meas. Tech.*, 6, 2607-2626, 10.5194/amt-6-2607-2013, 2013.

532 Choi, Y., and Souri, A. H.: Chemical condition and surface ozone in large cities of Texas during
533 the last decade: Observational evidence from OMI, CAMS, and model analysis, *Remote Sensing*
534 of Environment, 168, 90-101, 10.1016/j.rse.2015.06.026, 2015.

535 Cooper, O. R., Gao, R.-S., Tarasick, D., Leblanc, T., and Sweeney, C.: Long-term ozone trends
536 at rural ozone monitoring sites across the United States, 1990-2010, *Journal of Geophysical*
537 *Research: Atmospheres*, 117, n/a-n/a, 10.1029/2012jd018261, 2012.

538 Duncan, B. N., Yoshida, Y., Olson, J. R., Sillman, S., Martin, R. V., Lamsal, L., Hu, Y.,
539 Pickering, K. E., Retscher, C., Allen, D. J., and Crawford, J. H.: Application of OMI
540 observations to a space-based indicator of NO_x and VOC controls on surface ozone formation,
541 *Atmospheric Environment*, 44, 2213-2223, 10.1016/j.atmosenv.2010.03.010, 2010.

542 Duncan, B. N., Lamsal, L. N., Thompson, A. M., Yoshida, Y., Lu, Z. F., Streets, D. G., Hurwitz,
543 M. M., and Pickering, K. E.: A space-based, high-resolution view of notable changes in urban
544 NO_x pollution around the world (2005-2014), *Journal of Geophysical Research-Atmospheres*,
545 121, 976-996, 10.1002/2015jd024121, 2016.

546 EPA: National Ambient Air Quality Standards for Ozone, *Federal Register*, 80, 2015.

547 Faloon, I. C., Tan, D., Leshner, R. L., Hazen, N. L., Frame, C. L., SImpas, J. B., Harder, G.,
548 Martinez, M., Di Carlo, P., Ren, X., and Brune, W. H.: A Laser-induced Fluorescence Instrument
549 for Detecting Tropospheric OH and HO₂: Characteristics and Calibration, *Journal of*
550 *Atmospheric Chemistry*, 47, 139-167, 2004.

551 González Abad, G., Liu, X., Chance, K., Wang, H., Kurosu, T. P., and Suleiman, R.: Updated
552 Smithsonian Astrophysical Observatory Ozone Monitoring Instrument (SAO OMI)
553 formaldehyde retrieval, *Atmospheric Measurement Techniques*, 8, 19-32, 10.5194/amt-8-19-
554 2015, 2015.

555 He, H., Stehr, J. W., Hains, J. C., Krask, D. J., Doddridge, B. G., Vinnikov, K. Y., Canty, T. P.,
556 Hosley, K. M., Salawitch, R. J., Worden, H. M., and Dickerson, R. R.: Trends in emissions and
557 concentrations of air pollutants in the lower troposphere in the Baltimore/Washington airshed
558 from 1997 to 2011, *Atmospheric Chemistry and Physics*, 13, 7859-7874, 10.5194/acp-13-7859-
559 2013, 2013.



- 560 Herndon, S. C., Jayne, J. T., Zahniser, M. S., Worsnop, D. R., Knighton, B., Alwine, E., Lamb,
561 B. K., Zavala, M., Nelson, D. D., McManus, J. B., Shorter, J. H., Canagaratna, M. R., Onasch, T.
562 B., and Kolb, C. E.: Characterization of urban pollutant emission fluxes and ambient
563 concentration distributions using a mobile laboratory with rapid response instrumentation,
564 *Faraday Discussions*, 130, 327-339, 10.1039/b500411j, 2005.
- 565 Holton, J. R., Haynes, P. H., McIntyre, M. E., Douglass, A. R., Rood, R. B., and Pfister, L.:
566 *Stratosphere-Troposphere Exchange*, *Reviews of Geophysics*, 33, 403-439, 1995.
- 567 Jerrett, M., Burnett, R. T., Pope, C. A., Ito, K., Thurston, G., Krewski, D., Shi, Y. L., Calle, E.,
568 and Thun, M.: Long-Term Ozone Exposure and Mortality, *New England Journal of Medicine*,
569 360, 1085-1095, 10.1056/NEJMoa0803894, 2009.
- 570 Kebabian, P. L., Herndon, S. C., and Freedman, A.: Detection of Nitrogen Dioxide by Cavity
571 Attenuated Phase Shift Spectroscopy, *Analytical Chemistry*, 77, 724-728, 10.1029/, 2005.
- 572 Kebabian, P. L., Wood, E. C., Herndon, S. C., and Freedman, A.: A Practical Alternative to
573 Chemiluminescence-Based Detection of Nitrogen Dioxide: Cavity Attenuated Phase Shift
574 Spectroscopy, *Environmental Science & Technology*, 42, 6040-6045, 2008.
- 575 Kleinman, L. I.: Low and High NO_x Tropospheric Photochemistry, *Journal of Geophysical*
576 *Research-Atmospheres*, 99, 16831-16838, 10.1029/94jd01028, 1994.
- 577 Kleinman, L. I., Daum, P. H., Imre, D., Lee, Y. N., Nunnermacker, L. J., Springston, S. R.,
578 Weinstein-Lloyd, J., and Rudolph, J.: Ozone production rate and hydrocarbon reactivity in 5
579 urban areas: A cause of high ozone concentration in Houston, *Geophysical Research Letters*, 29,
580 105-101-105-104, 10.1029/2001gl014569, 2002.
- 581 Kleinman, L. I.: The dependence of tropospheric ozone production rate on ozone precursors,
582 *Atmospheric Environment*, 39, 575-586, 10.1016/j.atmosenv.2004.08.047, 2005.
- 583 Krotkov, N. A., Lamsal, L. N., Celarier, E. A., Swartz, W. H., Marchenko, S. V., Bucsel, E. J.,
584 Chan, K. L., Wenig, M., and Zara, M.: The version 3 OMI NO₂ standard product, *Atmospheric*
585 *Measurement Techniques*, 10, 3133-3149, 10.5194/amt-10-3133-2017, 2017.
- 586 Kundu, S., Deming, B., Lew, M., Bottorff, B., Stevens, P.S., Dusanter, S., Sklaveniti, S.,
587 Leonardis, T., Locoge, N., and Wood, E.: Peroxy Radical Measurements by Ethane - Nitric
588 Oxide Chemical Amplification (ECHAMP) and Laser-Induced Fluorescence/Fluorescence Assay
589 by Gas Expansion (LIF-FAGE) during the IRRONIC field campaign in a Forest in Indiana, in
590 preparation.
- 591 Lamarque, J. F., Hess, P., Emmons, L., Buja, L., Washington, W., and Granier, C.: Tropospheric
592 ozone evolution between 1890 and 1990, *Journal of Geophysical Research-Atmospheres*, 110,
593 10.1029/2004jd005537, 2005.
- 594 Lamsal, L. N., Duncan, B. N., Yoshida, Y., Krotkov, N. A., Pickering, K. E., Streets, D. G., and
595 Lu, Z. F.: U.S. NO₂ trends (2005-2013): EPA Air Quality System (AQS) data versus improved



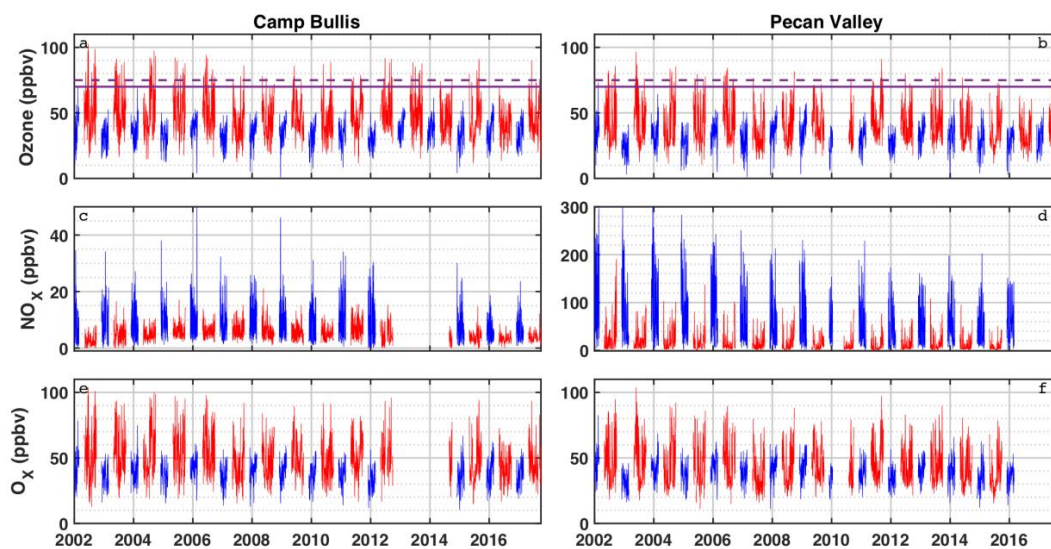
- 596 observations from the Ozone Monitoring Instrument (OMI), *Atmospheric Environment*, 110,
597 130-143, 10.1016/j.atmosenv.2015.03.055, 2015.
- 598 Lee, B. H., Wood, E. C., Herndon, S. C., Lefer, B. L., Luke, W. T., Brune, W. H., Nelson, D. D.,
599 Zahniser, M. S., and Munger, J. W.: Urban measurements of atmospheric nitrous acid: A caveat
600 on the interpretation of the HONO photostationary state, *Journal of Geophysical Research:*
601 *Atmospheres*, 118, 12,274-212,281, 10.1002/2013jd020341, 2013.
- 602 Mao, J. Q., Ren, X., Chen, S., Brune, W. H., Chen, Z., Martinez, M., Harder, H., Lefer, B.,
603 Rappenglück, B., Flynn, J., and Leuchner, M.: Atmospheric oxidation capacity in the summer of
604 Houston 2006: Comparison with summer measurements in other metropolitan studies,
605 *Atmospheric Environment*, 44, 4107-4115, 10.1016/j.atmosenv.2009.01.013, 2010.
- 606 Mazzuca, G. M., Ren, X., Loughner, C. P., Estes, M., Crawford, J. H., Pickering, K. E.,
607 Weinheimer, A. J., and Dickerson, R. R.: Ozone production and its sensitivity to NO_x and
608 VOCs: results from the DISCOVER-AQ field experiment, Houston 2013, *Atmospheric*
609 *Chemistry and Physics*, 16, 14463-14474, 10.5194/acp-16-14463-2016, 2016.
- 610 McManus, J. B., Zahniser, M. S., Nelson, D. D., Shorter, J. H., Herndon, S. C., Jervis, D.,
611 Agnese, M., McGovern, R., Yacovitch, T. I., and Roscioli, J. R.: Recent progress in laser-based
612 trace gas instruments: performance and noise analysis, *Applied Physics B-Lasers and Optics*,
613 119, 203-218, 10.1007/s00340-015-6033-0, 2015.
- 614 Mihele, C. M., and Hastie, D. R.: Optimized operation and calibration procedures for radical
615 amplifier-type detectors, *Journal of Atmospheric and Oceanic Technology*, 17, 788-794,
616 10.1175/1520-0426(2000)017<0788:Ooacpf>2.0.Co;2, 2000.
- 617 Orlando, J. J., and Tyndall, G. S.: Laboratory studies of organic peroxy radical chemistry: an
618 overview with emphasis on recent issues of atmospheric significance, *Chemical Society*
619 *Reviews*, 41, 6294-6317, 10.1039/c2cs35166h, 2012.
- 620 Park, S. K., O'Neill, M. S., Vokonas, P. S., Sparrow, D., and Schwartz, J.: Effects of air pollution
621 on heart rate variability: The VA Normative Aging Study, *Environmental Health Perspectives*,
622 113, 304-309, 10.1289/ehp.7447, 2005.
- 623 Pollack, I. B., Ryerson, T. B., Trainer, M., Parrish, D. D., Andrews, A. E., Atlas, E. L., Blake, D.
624 R., Brown, S. S., Commane, R., Daube, B. C., de Gouw, J. A., Dubé, W. P., Flynn, J., Frost, G.
625 J., Gilman, J. B., Grossberg, N., Holloway, J. S., Kofler, J., Kort, E. A., Kuster, W. C., Lang, P.
626 M., Lefer, B., Lueb, R. A., Neuman, J. A., Nowak, J. B., Novelli, P. C., Peischl, J., Perring, A.
627 E., Roberts, J. M., Santoni, G., Schwarz, J. P., Spackman, J. R., Wagner, N. L., Warneke, C.,
628 Washenfelder, R. A., Wofsy, S. C., and Xiang, B.: Airborne and ground-based observations of a
629 weekend effect in ozone, precursors, and oxidation products in the California South Coast Air
630 Basin, *Journal of Geophysical Research: Atmospheres*, 117, n/a-n/a, 10.1029/2011jd016772,
631 2012.
- 632 Pollmann, J., Helmig, D., Hueber, J., Tanner, D., and Tans, P. P.: Evaluation of solid adsorbent
633 materials for cryogen-free trapping - gas chromatographic analysis of atmospheric C₂-C₆ non-



- 634 methane hydrocarbons, *Journal of Chromatography A*, 1134, 1-15,
635 10.1016/j.chroma.2006.08.050, 2006.
- 636 Ren, X., van Duin, D., Cazorla, M., Chen, S., Mao, J., Zhang, L., Brune, W. H., Flynn, J. H.,
637 Grossberg, N., Lefer, B. L., Rappenglück, B., Wong, K. W., Tsai, C., Stutz, J., Dibb, J. E.,
638 Thomas Jobson, B., Luke, W. T., and Kelley, P.: Atmospheric oxidation chemistry and ozone
639 production: Results from SHARP 2009 in Houston, Texas, *Journal of Geophysical Research:*
640 *Atmospheres*, 118, 5770-5780, 10.1002/jgrd.50342, 2013.
- 641 Ring, A. M., Canty, T. P., Anderson, D. C., Vinciguerra, T. P., He, H., Goldberg, D. L., Ehrman,
642 S. H., Dickerson, R. R., and Salawitch, R. J.: Evaluating commercial marine emissions and their
643 role in air quality policy using observations and the CMAQ model, *Atmospheric Environment*,
644 173, 96-107, 10.1016/j.atmosenv.2017.10.037, 2018.
- 645 Ryerson, T. B., Trainer, M., Angevine, W. M., Brock, C. A., Dissly, R. W., Fehsenfeld, F. C.,
646 Frost, G. J., Goldan, P. D., Holloway, J. S., Hubler, G., Jakoubek, R. O., Kuster, W. C., Neuman,
647 J. A., Nicks, D. K., Parrish, D. D., Roberts, J. M., Sueper, D. T., Atlas, E. L., Donnelly, S. G.,
648 Flocke, F., Fried, A., Potter, W. T., Schauffler, S., Stroud, V., Weinheimer, A. J., Wert, B. P.,
649 Wiedinmyer, C., Alvarez, R. J., Banta, R. M., Darby, L. S., and Senff, C. J.: Effect of
650 petrochemical industrial emissions of reactive alkenes and NO_x on tropospheric ozone formation
651 in Houston, Texas, *Journal of Geophysical Research-Atmospheres*, 108, 10.1029/2002jd003070,
652 2003.
- 653 Sanchez, J., Tanner, D. J., Chen, D., Huey, L. G., and Ng, N. L.: A new technique for the direct
654 detection of HO₂ radicals using bromide chemical ionization mass spectrometry (Br-CIMS):
655 initial characterization, *Atmospheric Measurement Techniques*, 9, 3851-3861, 10.5194/amt-9-
656 3851-2016, 2016.
- 657 Schade, G. W., and Roest, G.: Analysis of non-methane hydrocarbon data from a monitoring
658 station affected by oil and gas development in the Eagle Ford shale, Texas, *Elementa: Science of*
659 *the Anthropocene*, 4, 10.12952/journal.elementa.000096, 2016.
- 660 Schroeder, J. R., Crawford, J. H., Fried, A., Walega, J., Weinheimer, A., Wisthaler, A., Müller,
661 M., Mikoviny, T., Chen, G., Shook, M., Blake, D. R., and Tonnesen, G. S.: New insights into the
662 column CH₂O/NO₂ ratio as an indicator of near-surface ozone sensitivity, *Journal of Geophysical*
663 *Research: Atmospheres*, 10.1002/2017jd026781, 2017.
- 664 Shetter, R. E., Junkermann, W., Swartz, W. H., Frost, G. J., Crawford, J. H., Lefer, B. L.,
665 Barrick, J. D., Hall, S. R., Hofzumahaus, A., Bais, A., Calvert, J. G., Cantrell, C. A., Madronich,
666 S., Muller, M., Kraus, A., Monks, P. S., Edwards, G. D., McKenzie, R., Johnston, P., Schmitt,
667 R., Griffioen, E., Krol, M., Kylling, A., Dickerson, R. R., Lloyd, S. A., Martin, T., Gardiner, B.,
668 Mayer, B., Pfister, G., Roth, E. P., Koepke, P., Ruggaber, A., Schwander, H., and van Weele,
669 M.: Photolysis frequency of NO₂: Measurement and modeling during the International
670 Photolysis Frequency Measurement and Modeling Intercomparison (IPMMI), *Journal of*
671 *Geophysical Research-Atmospheres*, 108, 10.1029/2002jd002932, 2003.
- 672 Silva, R. A., West, J. J., Zhang, Y., Anenberg, S. C., Lamarque, J.-F., Shindell, D. T., Collins,
673 W. J., Dalsoren, S., Faluvegi, G., Folberth, G., Horowitz, L. W., Nagashima, T., Naik, V.,



- 674 Rumbold, S., Skeie, R., Sudo, K., Takemura, T., Bergmann, D., Cameron-Smith, P., Cionni, I.,
675 Doherty, R. M., Eyring, V., Josse, B., MacKenzie, I. A., Plummer, D., Righi, M., Stevenson, D.
676 S., Strode, S., Szopa, S., and Zeng, G.: Global premature mortality due to anthropogenic outdoor
677 air pollution and the contribution of past climate change, *Environmental Research Letters*, 8,
678 034005, 10.1088/1748-9326/8/3/034005, 2013.
- 679 Sommariva, R., Brown, S. S., Roberts, J. M., Brookes, D. M., Parker, A. E., Monks, P. S., Bates,
680 T. S., Bon, D., de Gouw, J. A., Frost, G. J., Gilman, J. B., Goldan, P. D., Herndon, S. C., Kuster,
681 W. C., Lerner, B. M., Osthoff, H. D., Tucker, S. C., Warneke, C., Williams, E. J., and Zahniser,
682 M. S.: Ozone production in remote oceanic and industrial areas derived from ship based
683 measurements of peroxy radicals during TexAQS 2006, *Atmospheric Chemistry and Physics*, 11,
684 2471-2485, 10.5194/acp-11-2471-2011, 2011.
- 685 Stark, H., Lerner, B. M., Schmitt, R., Jakoubek, R., Williams, E. J., Ryerson, T. B., Sueper, D.
686 T., Parrish, D. D., and Fehsenfeld, F. C.: Atmospheric in situ measurement of nitrate radical
687 (NO_3) and other photolysis rates using spectroradiometry and filter radiometry, *Journal of*
688 *Geophysical Research-Atmospheres*, 112, 10.1029/2006jd007578, 2007.
- 689 Thornton, J. A.: Ozone production rates as a function of NO_x abundances and HO_x production
690 rates in the Nashville urban plume, *Journal of Geophysical Research*, 107,
691 10.1029/2001jd000932, 2002.
- 692 Whalley, L. K., Stone, D., Dunmore, R., Hamilton, J., Hopkins, J. R., Lee, J. D., Lewis, A. C.,
693 Williams, P., Kleffmann, J., Laufs, S., Woodward-Massey, R., and Heard, D. E.: Understanding
694 in situ ozone production in the summertime through radical observations and modelling studies
695 during the Clean air for London project (ClearfLo), *Atmospheric Chemistry and Physics*, 18,
696 2547-2571, 10.5194/acp-18-2547-2018, 2018.
- 697 Wolfe, G. M., Kaiser, J., Hanisco, T. F., Keutsch, F. N., de Gouw, J. A., Gilman, J. B., Graus,
698 M., Hatch, C. D., Holloway, J., Horowitz, L. W., Lee, B. H., Lerner, B. M., Lopez-Hilifiker, F.,
699 Mao, J., Marvin, M. R., Peischl, J., Pollack, I. B., Roberts, J. M., Ryerson, T. B., Thornton, J. A.,
700 Veres, P. R., and Warneke, C.: Formaldehyde production from isoprene oxidation across NO_x
701 regimes, *Atmospheric Chemistry and Physics*, 16, 2597-2610, 10.5194/acp-16-2597-2016,
702 2016a.
- 703 Wolfe, G. M., Marvin, M. R., Roberts, S. J., Travis, K. R., and Liao, J.: The Framework for 0-D
704 Atmospheric Modeling (F0AM) v3.1, *Geosci. Model Dev.*, 9, 3309-3319, 10.5194/gmd-9-3309-
705 2016, 2016b.
- 706 Wood, E. C., Deming, B. L., and Kundu, S.: Ethane-Based Chemical Amplification
707 Measurement Technique for Atmospheric Peroxy Radicals, *Environmental Science &*
708 *Technology Letters*, 4, 15-19, 10.1021/acs.estlett.6b00438, 2017.
709



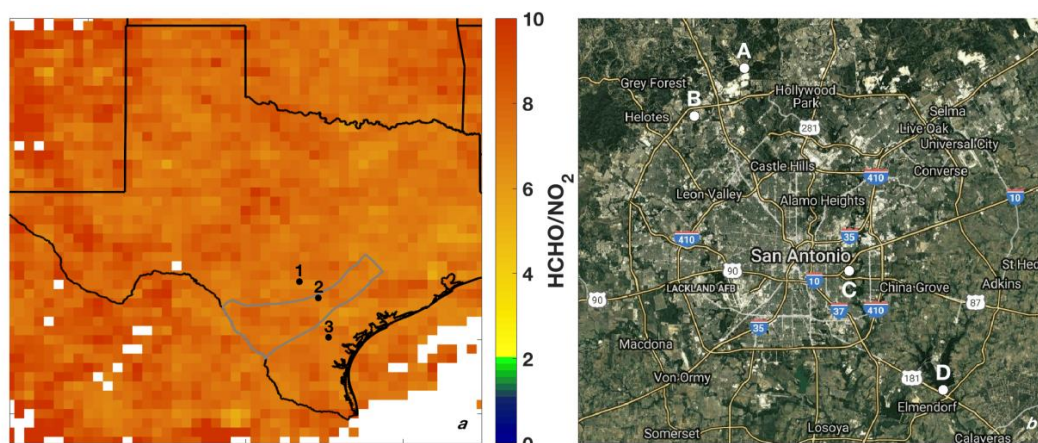
710

711 **Figure 1:** Time series of maximum daily average 8-hour (MDA8) O₃, NO_x, and O_x at the Camp
712 Bullis (a, c, e) and Pecan Valley (b, d, f) TCEQ sites for 2002 – 2017. Summer months (May –
713 September) are shown in red, and winter months (December – February) are shown in blue. MDA8
714 is calculated by determining the maximum value of a species from running 8 hour averages
715 throughout the day. The purple dashed and solid red lines represent the 2008 (75 ppbv) and 2015
716 (70 ppbv) O₃ standards respectively. Data were downloaded from
717 www.tceq.texas.gov/goto/tamis.



718

719



720

721

722

723

724

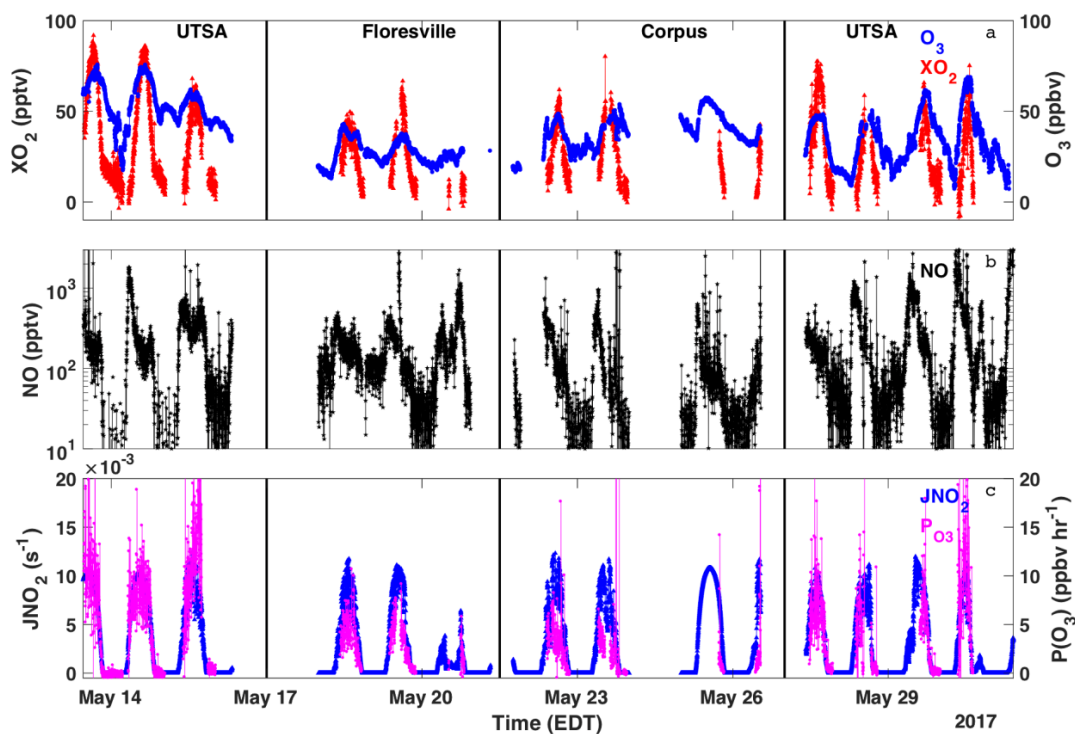
725

726

727

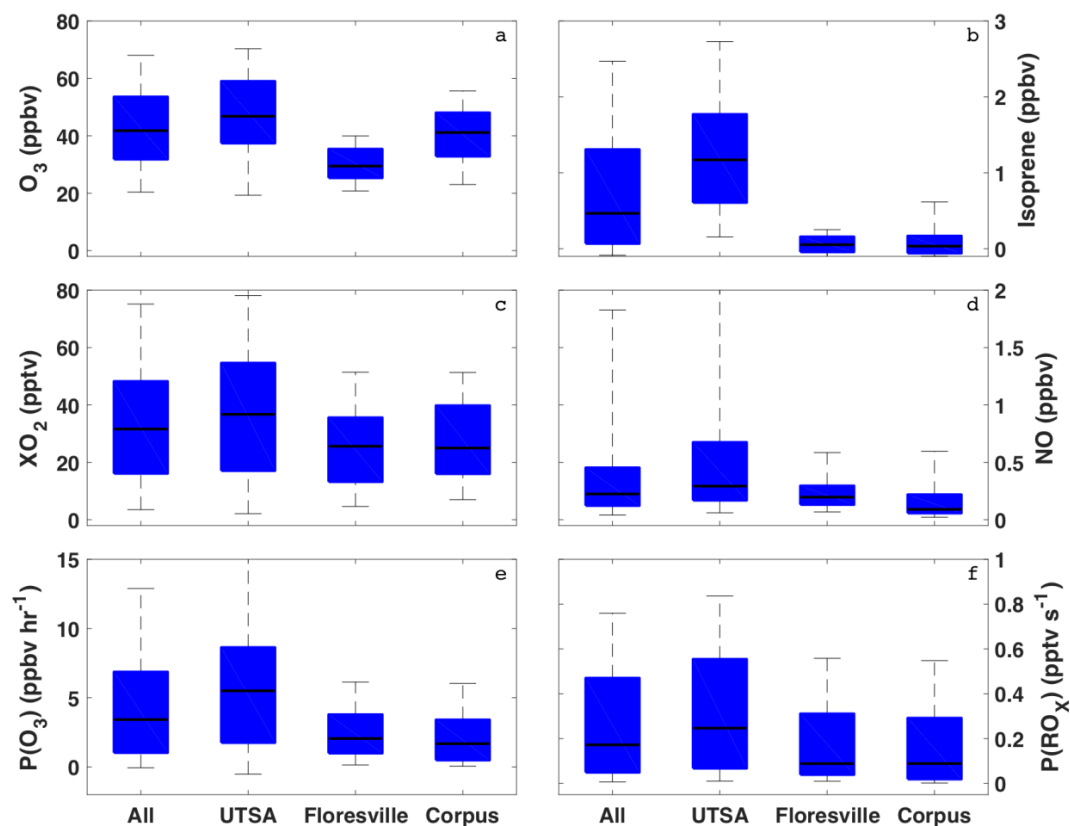
Figure 2: The sampling locations for the Aerodyne mobile laboratory are indicated: 1 – University of Texas San Antonio, 2 – Floresville, 3 – Lake Corpus Christi. The ratio of total column HCHO to tropospheric column NO₂ averaged over the months of May through July 2017 is also shown for grid boxes with 10 or more observations of both species over the indicated time period. The outline of the Eagle Ford Shale play is also shown for reference in grey. (b) The major roadways and TCEQ monitoring stations (A: Camp Bullis, C: Pecan Valley, D: Calaveras Lake) in the San Antonio region used in this study are shown. The UTSA SAFS site (B) is also shown for reference.

728



729

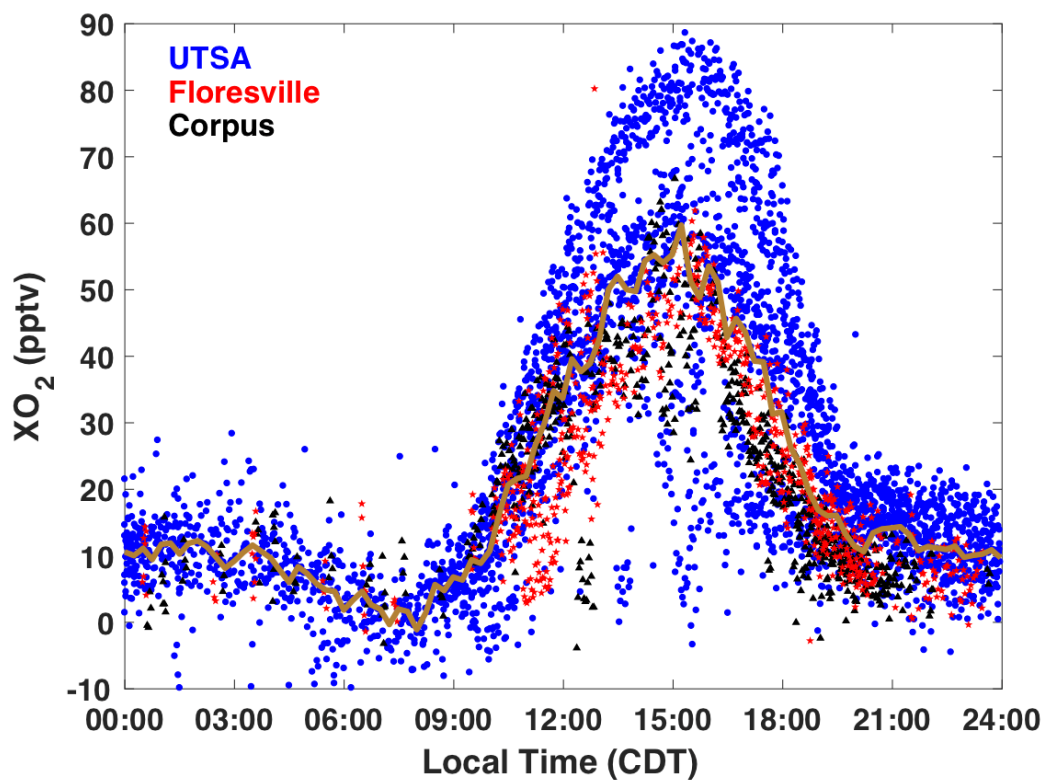
730 **Figure 3:** Time series of O₃ (blue circles), XO₂ (red triangles), NO (black stars), JNO₂ (blue triangles),
731 and P(O₃) (magenta circles) measured at all sites. All data are averaged over the XO₂ sampling period.



732

733 **Figure 4:** The distribution of O₃ (a), isoprene (b), XO₂ (c), NO (d), P(O₃) (e), and P(RO_x) (f) for all
734 observations during SAFS taken between 07:00 and 20:00. The distribution for the entire campaign (All)
735 as well as at the individual sites is shown. Medians are indicated by the black lines, and the 5th, 25th, 75th,
736 and 95th percentiles are shown by the edges of the box and whiskers.

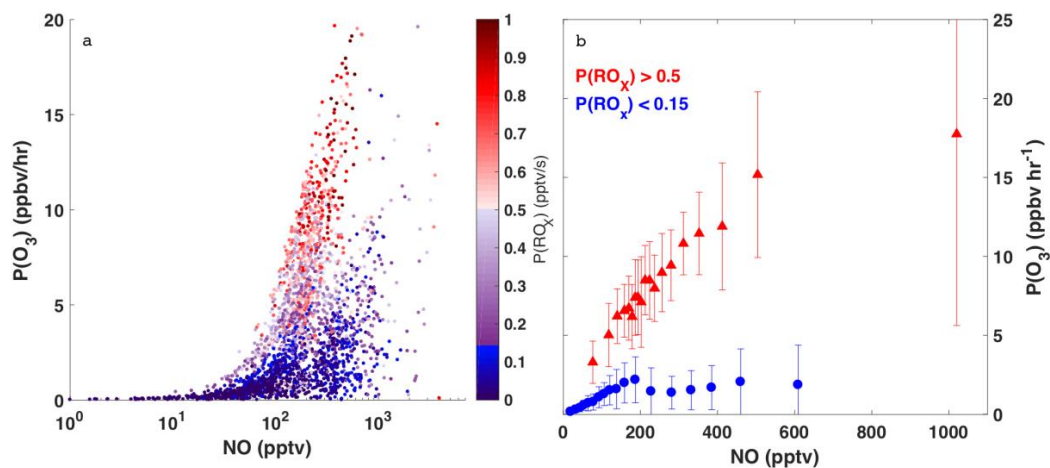
737



738

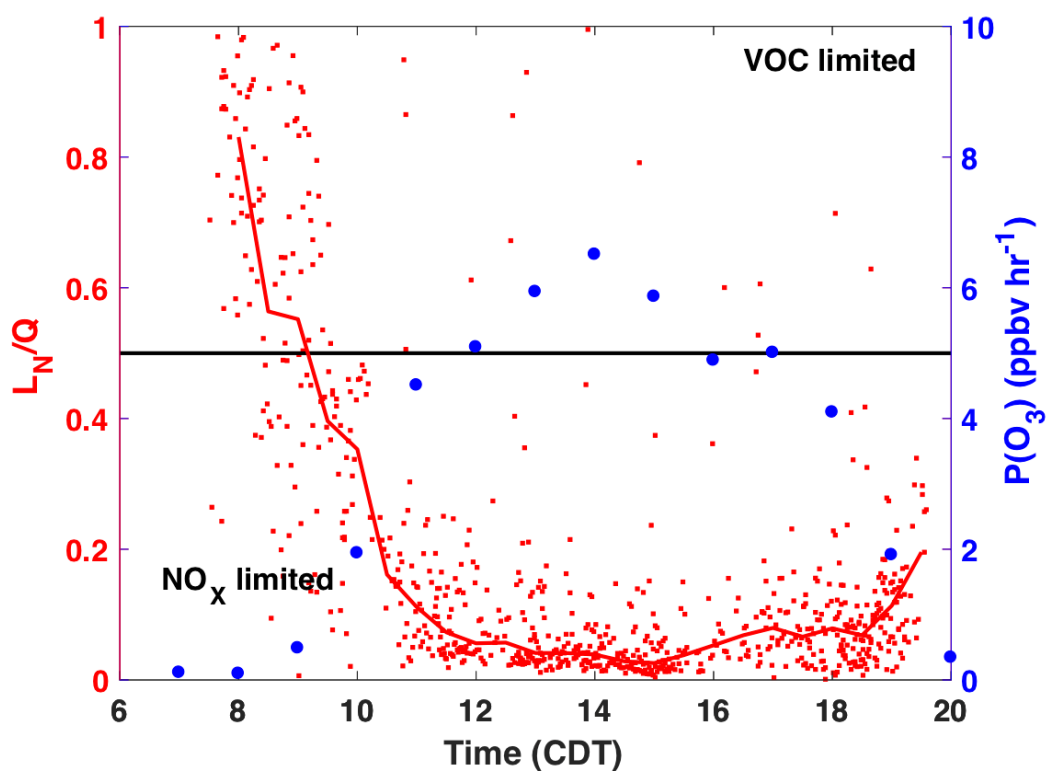
739 **Figure 5:** The diurnal profile of all 2 minute average XO_2 observations made during SAFS. Observations
740 made at UTSA are shown in blue, Floresville, in red, and Corpus, in black. The median value for 15-
741 minute time bins is shown by the gold trace.

742



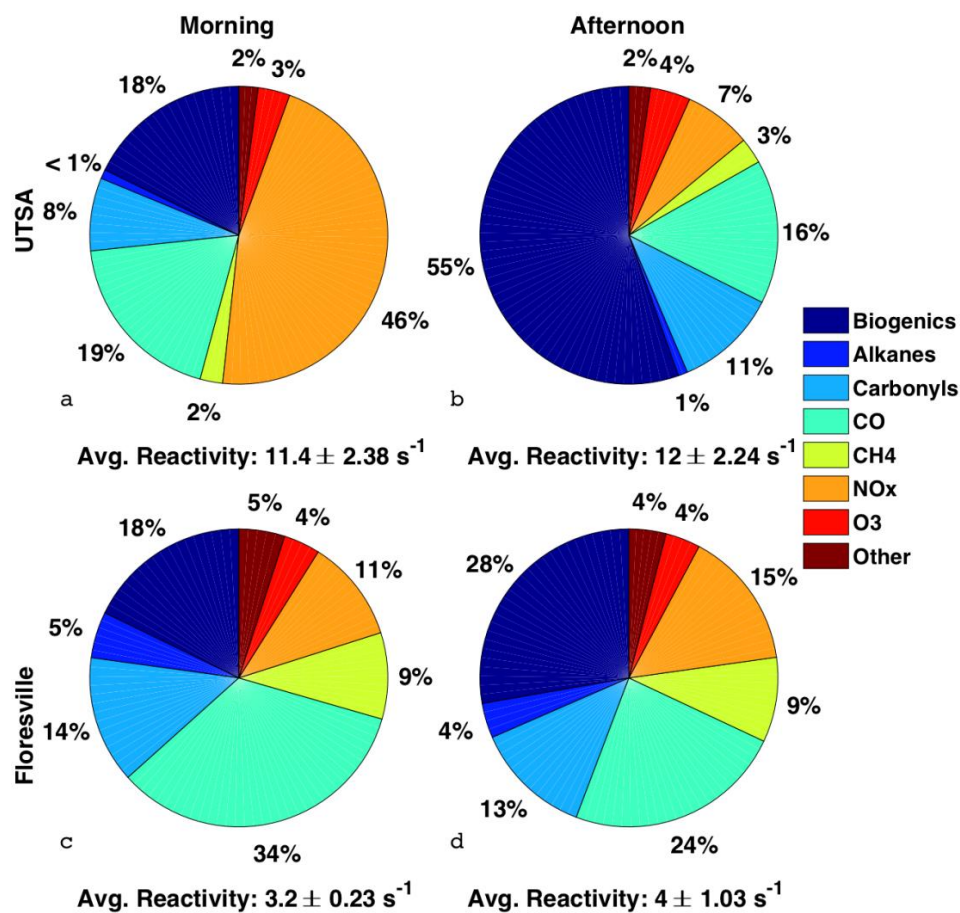
743

744 **Figure 6:** The variation of $P(\text{O}_3)$ with NO for all daytime observations (07:00 to 20:00) made during
745 SAFS (a). Observations are colored by $P(\text{RO}_x)$. The same data as shown in panel (a) but sorted by
746 $P(\text{RO}_x)$ are shown in panel (b). Observations with $P(\text{RO}_x)$ greater than 0.5 pptv s^{-1} are shown in red,
747 while observations with $P(\text{RO}_x)$ less than 0.15 pptv s^{-1} are shown in blue. Data are separated into NO
748 bins with an equal number of observations in bin. The mean value of each bin is shown, with the error
749 bars showing one standard deviation.



750

751 **Figure 7:** The diurnal profiles of L_N/Q calculated with the FOAM box model (red), and the median $P(O_3)$
752 in one hour time bins (blue). The median L_N/Q value for half hour bins is shown by the red line. Profiles
753 are only for observations at UTSA. Points are calculated by $P(O_3)$ calculated from observations. The
754 black line is approximately the separation between the NO_x - and VOC-limited regimes.



755

756 **Figure 8:** The distribution of the various contributors to the overall OH reactivity for the UTSA (13 -16
 757 May) and Floresville (17 – 19 May) sites are shown for both the morning, times between 7:00 and 11:00,
 758 and afternoon, times between 13:00 and 20:00. The average OH reactivity ($\pm 1\sigma$) is also shown.

759

760

761